IEEE Access
Multidisciplinary | Rapid Review | Open Access Journal

Received 24 June 2022, accepted 1 August 2022, date of publication 4 August 2022, date of current version 17 August 2022.

Digital Object Identifier 10.1109/ACCESS.2022.3196376

RESEARCH ARTICLE

In-vivo Experimental Validation of the Attenuation Path Loss Model for Localization of Wireless Implanted Transmitters at 2.45 GHz

YANA A. SALCHAK[1], (Graduate Student Member, IEEE), NOOR M. ALBADRI[1], TRACEY BJORKMAN[2], CORA LAU[3], ESMAEIL S. NADIMI[4], (Senior Member, IEEE), PETER BOLLEN[5], HUGO G. ESPINOSA[1], (Senior Member, IEEE), AND DAVID V. THIEL[1], (Life Senior Member, IEEE)

[1]School of Engineering and Built Environment, Griffith University, Brisbane, QLD 4111, Australia
[2]UQ Centre for Clinical Research, The University of Queensland, Brisbane, QLD 4072, Australia
[3]Biological Resources, The University of Queensland, Brisbane, QLD 4072, Australia
[4]Applied AI and Data Science, The Maersk Mc-Kinney Moeller Institute, University of Southern Denmark, 5230 Odense, Denmark
[5]Department of Experimental Medicine, University of Copenhagen, 2200 Copenhagen, Denmark

Corresponding author: Yana A. Salchak (iana.salchak@griffithuni.edu.au)

This work involved human subjects or animals in its research. Approval of all ethical and experimental procedures and protocols was granted by The University of Queensland Animal Ethics Committee under Approval No. UQCCR/GRIFFITH/406/20, the Danish Animal Inspectorate under License No. 2016-15-0201-00815, and the Institutional Animal Welfare Body (AWB), the equivalent of the Institutional Animal Care and Use Committee (IACUC), and performed in line with the Guidelines of ARRIVE.

ABSTRACT Wireless capsule endoscopy (WCE) is a modern, non-invasive method of gastrointestinal examination that can significantly reduce mortality and morbidity. One of the current challenges in WCE is the precise localization of the capsule. An accurate path loss propagation model can be used to find the exact distance from the surface to the capsule inside the abdominal cavity. Unfortunately, there are no standardized In-to-On-Body channel models describing the signal propagation at ultra-high frequencies that are used in the most commercially available WCE systems. This study addresses the gap by conducting an experimental validation of a new propagation model for WCE applications at 2.45 GHz. The results were confirmed by conducting two separate *in-vivo* trials on porcine animals under general anesthesia. The performance of the model as well as the corresponding ranging errors were evaluated when it was used as an inverse solution for distance estimation to an ingested transmitter. The main advantage of the model is its theoretical basis, which can help further generalize the findings for similar communication scenarios. The obtained ranging error was smaller than one centimeter, suggesting that it can be used for accurate range-based positioning of implanted transmitters.

INDEX TERMS Wireless communication, wireless capsule endoscopy, body area networks, channel models, implantable biomedical devices, animals, UHF antennas, narrowband.

I. INTRODUCTION

Significant advances in microelectronics and radio frequency (RF) communications have facilitated the implementation of wireless sensor networks in various fields. Depending on the application, a specific technology is required to describe the relevant communication channel. This study focuses on Wireless Body Area Networks (WBAN), which include communications between sensors in close proximity to or inside the human body. Wireless Body Area Network technology provides opportunities for creating innovative engineering solutions in areas such as entertainment, assisted living, and continuous health monitoring. Some of the most prominent areas of application are personalized medicine and smart healthcare. The benefits of WBAN systems have been reported in managing patients with chronic conditions, patients undergoing rehabilitation, and when creating novel diagnostic and treatment systems [1]. The latter includes

The associate editor coordinating the review of this manuscript and approving it for publication was Anandakumar Haldorai.

sophisticated implantable sensors tailored for a particular medical condition. For example, modern solutions in cardiovascular medicine enable control of the heart rate in patients with arrhythmia using on-demand pacemakers [2]. In neurological medicine, wireless sensor systems can identify oncoming seizures to provide timely drug delivery and alert physicians of an oncoming emergency [3], etc.

In gastrointestinal (GI) disease diagnostics, a novel method called wireless capsule endoscopy (WCE) was introduced in 2001 [4]. It consists of a battery-powered swallowable device with one or several cameras, a light source, and a radio transmitter (Tx). Wireless capsule endoscopy is a painless, non-invasive method for visual assessment of the GI tract that does not require sedation or the presence of medical staff during the examination. These advantages make WCE suitable for efficient screening of larger population groups, which can provide timely detection of abnormalities and significantly reduce mortality rates [5].

These and other medical applications of WBAN are based on the wireless transmission of relevant biological data obtained by the implanted sensors, while wearable antennas in close proximity to the patient's body act as the receivers. In WBAN, this is described as the in-body to on-body (in-to-on body) communication channels.

The design of any communication channel requires a reliable propagation path loss model (PLM). These models are often developed by IEEE communication standards, while the standards for WBAN also consider additional regulations of radiation exposure safety for human tissues. The most commonly accepted standard dedicated to in-to-on body communications is IEEE 802.15.6. This standard defines the application of a Medical Implant Communication Service (MICS) band of 402-405 MHz and suggests the log-normal shadowing model for path loss estimation [6]. The ongoing research in implantable system design reports communications at higher frequencies, including the Industrial, Scientific and Medical (ISM) band of 2.45 GHz and ultra-wideband (UWB; from 3.1 GHz to 10.6 GHz) [7]. Such frequencies enable higher data rate transmission while allowing for a smaller antenna size. This is particularly beneficial for WCE, because it uses small pills swallowed by the patient to record the video of the lining while peristalsis propagates the pill through the GI tract. The video data are transmitted to several receiving antennas on the skin of the patient distributed across the torso. Although the high quality of the image is important for the correct diagnosis and interpretation of the results [8], [9], current formulations do not provide reliable propagation models for WCE at higher RF-frequencies.

In RF communications, propagation models are primarily used to estimate the coverage and predict signal loss over a desired range of distances for link budget calculations. However, the reliability of these models can also influence the accuracy of any other applications that rely on the analysis of the received signal strength (RSS). For example, one of the most relevant challenges preventing WCE from broad clinical application is the inability to accurately locate the pill position along the GI tract. Implementation of localization methods based on RSS analysis for these purposes is considered a promising solution. RSS-indicator (RSSI)- based localization methods have a low susceptibility to bandwidth limitations and do not require time synchronization or any additional in-capsule circuit requirements, compared to other RF-based approaches [10]. They can use the same radio signal for both the localization and the video data transmission. The positioning principles in this case rely on a predefined relationship between the RSS and the distance to the Tx (pill) with an unknown location. This correspondence can be found using a channel propagation model or a PLM, and its accuracy directly affects the localization precision.

This paper reports an alternative in-to-on body propagation model developed to ensure precise WCE localization using the RSS. Validation of the proposed solution was performed for the ISM 2.45 GHz frequency band, a narrowband technique, using *in-vivo* experiments. To the best of our knowledge, this has not been reported previously.

A. IN-BODY COMMUNICATION MODELS

A common path loss PL propagation model is the log-distance model:

$$PL\,(d) = PL\,(d_0) + 10nlog_{10}\left(\frac{d}{d_0}\right), \tag{1}$$

where d is the path length between the transmitting (Tx) and the receiving antennas (Rx), $PL\ (d_0)$ is the path loss at a reference distance d_0, and n is the path loss exponent. The relationship originates from the Friis transmission formula for propagation in free space [11], while the path loss exponent n is included to adjust the result in accordance with the losses due to diffraction, scattering, and reflection specific to the environment. These effects can increase the exponent significantly. By performing numerous measurements in the same surroundings, it is possible to empirically determine path loss exponent values that guarantee statistically reliable performance of the model. Since conducting experiments in air is relatively easy, the corresponding path loss exponents for the most common propagation environments have been evaluated over the years and are currently well known and accepted for use in both outdoor and indoor communications [12]. Analysis of the signal propagation through the human body is more complex due to the additional signal loss caused by the absorption in soft tissues, which must be included in the model.

The human body consists of various visceral organs and soft tissues with unique conductivity and relative permittivity values that change depending on the frequency of the applied electromagnetic (EM) field. Thus, the PLM for WBAN communications must be developed and verified considering the EM characteristics of the environment and the specific operational frequency. At the same time, the validation of any engineering solution with medical applications is complicated by the inability to easily perform large numbers of experiments

on living humans. This is particularly true for technologies involving communications between an implanted transmitter and on-body receivers, such as the WCE systems. Commonly, numerical and physical phantoms are used to imitate the EM properties of human soft tissues as the propagation environment.

The PLM for communication between an implanted sensor and on-body receivers, described in the IEEE.802.15.6 standard, was developed based on the statistical analysis of the measurement data obtained through numerical modeling [13]. The path loss exponent values for the logarithmic model, similar to (1), were found based on extensive numerical simulations using a digital male model as a representation of the real human torso and chest areas. These simulations included only MICS frequencies. An additional shadowing term (a zero-mean Gaussian noise variable in dB) was included in (1) to represent the measurement uncertainty caused by the processes occurring in a living human. Although the high-definition discretized digital models were used to verify the PLM, the paper [13] stated that the results must be additionally validated through physical measurements.

Different experimentally obtained values of the PLM parameters at higher frequencies (ISM and UWB) have been reported in the literature [14]–[18]. The results demonstrated several mathematical models suggested for appropriate signal loss prediction, including linear, lognormal, and log-distance functions. There are significant discrepancies observed between research groups, even when the same frequency was chosen for the validation. This can be partly explained by the difference in the experimental methods used. In [14], [15], a flat phantom filled with a liquid simulating human muscle was used for the data acquisition, whereas in [17], a sucrose and sodium chloride solution in a cube-shaped container was used. Other papers report experiments on gelatin-based phantoms in the shape of a human body or *ex-vivo* animal tissue phantoms for investigating in-to-on body channels [19]–[21].

A major limitation of both digital models and physical phantoms is that they cannot fully represent the natural processes that occur in living humans, such as respiratory and digestive movements or the circulation of biological fluids. The most reliable representation of signal propagation in the human body is achieved when measurements are performed on living laboratory animals. Several types of animals have been used for these purposes. It has been reported that porcine animals provide an accurate representation of the ISM frequency band antenna performance when implanted in humans [22]. Although animal research can play a vital role in scientific investigations, ethical considerations may explain the limited number of results reported.

In-vivo experiments on anaesthetized porcine animals for path loss model validation were reported by [16] and [23] at UWB frequencies. In both cases, the log-distance PLM (1) parameters were validated. The path loss exponent n in this model is the sole parameter that describes the signal attenuation, which means that for different measurement equipment or a changing propagation environment, the reported parameters may no longer be appropriate. This was highlighted by [16]. In [23], different types of antennas were used, including patches and directive antennas, as on-body receivers. The different path loss exponent values were reported accordingly ($n = 8.03$ and $n = 7.20$ for the frequencies from 3.1 GHz to 5.1 GHz). An investigation of the dependency of the path loss exponent on the frequency in the test range from 1 GHz to 6 GHz [16] reported lower path losses at the lower frequencies. The correlation between the path loss exponent and the frequency values was described by a polynomial, developed based on the experimentally fitted parameters. This may not be applicable to an arbitrary channel configuration and was only used to highlight the difference in the signal loss at different frequencies.

In this paper, we report an *in-vivo* validation of an alternative propagation model that combines EM propagation theory and large-scale modeling principles (1) common in RF communications. The strong theoretical foundation of this formulation provides opportunities for further generalization. The simplicity of the analytical approximations shows that the model can be easily adjusted to other channel configurations, other operational frequencies, and different propagation path EM properties. The validation on living animals through two separate trials presented in the paper provides the most reliable experimental conditions, making the results sufficient to be considered for implementation in channel modelling in similar propagation environments.

The paper is organized as follows: Section II describes the attenuation path loss model (APLM) suggested for the validation in this paper and includes similar results reported in the literature. Section III describes the methodology of the experiments undertaken as well as the characteristics of the antennas used in the study. Two separate *in-vivo* trials were conducted using a cavity-backed slot antenna at 2.45 GHz as a receiver and an implanted inverted-F antenna as a Tx, imitating a commercial wireless capsule. Section IV discusses the results of the measurements and performance of the APLM. The accuracy and reliability were assessed by the corresponding variation in predicted RSSI in dB and the relative ranging error in millimeters. The latter served as a prediction of the possible localization accuracy associated with the use of the APLM. If the model is sufficiently accurate, it can be used to calculate the exact distances and find unknown locations of the implanted Tx using range-based positioning. Section V concludes the paper and suggests future research directions.

II. PATH LOSS MODEL INCLUDING SIGNAL ATTENUATION IN LOSSY MEDIA

A. RELATED WORK

The main characteristic describing plane EM wave propagation in lossy media is the attenuation constant α, which is defined by the EM properties of the environment for a fixed

TABLE 1. EM Properties of the Human Abdominal tissues at 2.45 ISM Band (Based on [28]).

Organ	Relative permittivity	Conductivity, [S/m]	Attenuation Coefficient, α (Np/m)
Colon	53.88	2.04	51.82
Small Intestine	54.43	3.17	79.29
Stomach Duodenum	62.16	2.21	52.38
Kidney	52.74	2.43	62.16
Muscle	52.73	1.74	44.78
Liver	43.04	1.69	47.94
Fat	5.28	0.11	8.18

angular frequency ω [24]:

$$\alpha = \omega \left[\frac{\mu\varepsilon'}{2} \left[\sqrt{1 + \left(\frac{\varepsilon''}{\varepsilon'} \right)^2} - 1 \right] \right]^{1/2}, \tag{2}$$

where ω is the angular frequency of the signal ($\omega = 2\pi f$), ε' is the real part of the complex relative permittivity and it is a measure of how much energy from an external electric field is stored in a material (it is equal to the absolute permittivity ε); ε'' is the imaginary part or loss factor – a measure of the dissipation or loss in the material. The attenuation constants for different human organs at 2.45 GHz are given in Table 1.

An investigation of alternative path loss propagation models that include the attenuation constant α rather than the path loss exponent n was presented in [14]. It reported experimental validation at 2.45 GHz on a homogenous physical phantom with EM properties mimicking human muscle tissue. The following linear PLM was used:

$$PL = \alpha d \left(10 log_{10} e^2 \right) + C, \tag{3}$$

where α is the attenuation constant measured in (1/cm or Np/m), and C is a constant in dB independent of distance. The reported results for the attenuation constant values determined from their experiments are given in Table 2. A comparison of the results and the analytical calculations in accordance with (2) was also discussed in the paper [14]. However, their experiments were designed for two insulated dipoles, both located inside the lossy medium (in-to-in body communication). The authors demonstrated the influence of the EM properties of the medium on the *PL* and proposed an empirically derived mathematical model to adjust the *PL* predictions for a particular tissue type. This was used to investigate the signal path loss in a heterogeneous medium [25]. For the in-to-on-body scenario, only the heterogeneous model was considered, which required a complicated path loss model that includes reflection coefficient values at each tissue boundary. No *in-vivo* validation of the model was reported for this model.

The attenuation constant α characterizes the signal attenuation in a lossy medium caused by dissipation as heat. In WCE, the wave is produced by an equivalent point source, such as a small antenna, which causes the signal propagation in the form of a spherical wave. In this case, the attenuation is largely influenced by the distance travelled and decreases in accordance with the inverse square law. Both these factors must be considered for the development of a reliable PLM. This idea was previously suggested when describing a novel WCE communication system design [26]. The following equation was considered for the path loss calculations:

$$\frac{P_r}{P_t} = \left(\frac{\lambda_{eff}}{4\pi R} \right)^2 G_t G_r (e^{-\alpha R})^2 \tag{4}$$

where P_t is the power transmitted, P_r is the power received, R is the distance between the transmitter and receiver; λ_{eff} is the wavelength in the material; G_t and G_r are the gains of the receiver and transmitter respectively; and α is the attenuation constant. Although the path loss model's general formulation was described in [26], the experimental validation was not provided because the paper focused on a novel implantable antenna design for WCE.

Our paper discusses a model similar to (4), hereafter the attenuation path loss model or APLM, and provides its experimental validation.

B. ATTENUATION PATH LOSS MODEL

The approach was previously tested numerically as an efficient algorithm for surface electric field reconstruction [27]. According to the attenuation-based solution suggested in the paper, the power of the surface electric field measured in dB from an implanted transmitter can be found as:

$$P = 20\log(E_0 \frac{e^{-\alpha R}}{R} \sin\theta), \tag{5}$$

where R is the distance between the Tx and the on-body receivers, E_0 is the radiated electric field from the Tx or an electric field measured at some reference distance R_0, α is the attenuation constant and θ represents the angle between the Tx approximated as a Hertzian dipole and the Rx position on the surface. An elliptical cylinder approximation of a human body with the averaged EM characteristics of the soft tissues in the GI tract was used for the simulations. The study presented in [27] included a comparison of the obtained results with the corresponding numerical simulations using a FIT-solver (CST Studio ®). A close agreement between them was demonstrated, while the proposed attenuation algorithm was significantly less computationally demanding.

In the experimental validation presented in the current research, a linearized version of (5) was used. For the measurements, an antenna acting as the EM field Tx was implanted into the abdominal cavity of living laboratory animals. Due to the high conductivity and permittivity of the

TABLE 2. Parameters of the selected in-body path loss propagation models at 2.45 ISM band.

Ref. Numb	Frequency, Scenario	Path loss propagation model	Parameters	Validation
[14]	2.45 GHz, In-to-In Body	Linear (plane wave): $PL\ (dB) = \alpha_1 d(10log_{10}e^2) + C_1(dB)$; $PL\ (dB) = \alpha_2 d(10log_{10}e^2) + C_2(dB)$;	α_1= 0.87 [1/cm] α_2= 0.67 [1/cm] C_1 = 8.93 C_2 = 14.10	Simulation; Physical muscle tissue phantom
[15]			α_1= 0.99 [1/cm] α_2= 0.66 [1/cm] C_1 = 7.18 C_2 = 15.79	
[16]	1-6 GHz, In-to-On Body	Log-distance: $PL(dB) = PL_0(d_0) + 10nlog_{10}\left(\frac{d}{d_0}\right)$	For 2.45 GHz n = 10.6	In-vivo experiment

surrounding soft tissues, it was assumed that the antenna behaved as an omnidirectional Hertzian dipole (explained in more detail in Section III). The orientation of the Tx was constant, which guaranteed that the maximum radiation direction remained between the Tx and all Rx positions on the skin surface. This allowed the approximation of θ sin ≅1 for both *in-vivo* experiments. Further analysis of the experimental results was conducted to support the assumption. Using the attenuation-based algorithm (5), the path loss in dB is:

$$PL\ (R) = 20log_{10}\left(e^{\alpha R}\right) + 20log_{10}\ (R) = 8.68\alpha R + 20log_{10}\ (R)\ . \quad (6)$$

For the validation of the model accuracy, the comparison of the predicted and measured RSSI data were made rather than the path loss, which can be expressed at a certain distance as:

$$RSSI\ (R) = Pt - PL\ (R)\ , \quad (7)$$

where Pt is the transmitted power that can be represented by a constant defined by the system configuration and equipment characteristics ($Pt = 20\log_{10} E_0$). In the following analysis, the transmitter power as well as the gains of both antennas were assumed to be included in the parameter C (dB). Thus, the linearized APLM (in dB) used for the validation in this study can be rewritten:

$$RSSI\ (R) = C - 8.68\alpha R - 20log_{10}R. \quad (8)$$

A comparison was also made with the results reported for the same frequency when using the most relevant models reported in the literature. Table 2 summarizes the models and the parameters used in the analysis in accordance with the related work for WCE applications outlined in Section II.A. The most similar approach and channel configuration were given in the initial experiments performed by [14], [15] at 2.45 GHz for a homogenous phantom. They were the only group that included a theoretical estimation of α based on the EM properties of the tissues. However, their experiments were designed for in-to-in body communication only and did not include *in-vivo* validation. The *in-vivo* experiment that included the 2.45 GHz frequency was conducted in [16]. The PLM used in their study was also considered for the comparison with the results obtained in the current paper. No specific values of the path loss exponent were given in [16], but in accordance with the presented model it could be estimated at $n = 10.6$ for the frequency of 2.45 GHz.

The performance of the APLM was tested against the results obtained when the two aforementioned PLMs were fitted to the same experimental data. For these purposes, (1) and (3) were used in the linearized form representing these models as RSSI functions, which depend on the separation distance (R):

$$RSSI\ (R) = C_2 - 10nlog_{10}\ (R)\ , \quad (9)$$

$$RSSI\ (R) = C_3 - 8.68\alpha R. \quad (10)$$

Equation 9 hereafter is referred to as the log-distance model, and (10) is referred to as the linear (plane wave) model. To validate the reliability of the study further, the parameters of these models were estimated and compared to the reported results (Table 2).

The Gauss-Newton Nonlinear Least Squares optimization method was used to obtain the best-fit parameters for each of the path loss propagation models tested in the current study.

III. METHODOLOGY

A. EXPERIMENTAL PROTOCOLS AND EQUIPMENT

Two experiments were conducted on anesthetized pigs. They involved the implantation of a small transmitter in the abdominal cavity of the animal and registering the received signal strength at multiple fixed positions on the skin surface distributed across the torso.

The first *in-vivo* experiment (Experiment 1) was conducted at the animal surgical facility of the University of Southern Denmark (SDU, Odense, Denmark), with the participation of trained medical staff under the Ethics Approval (Danish Animal Inspectorate under license 2016-15-0201-00815). A medium-sized domestic pig (approximately 45 kg, Yorkshire/Landrace cross, 88.5 cm waist circumference lying on its back) was intubated after premedication with sedatives (midazolam 0.25 mg/kg, medetomidin 0.03 mg/kg, ketamin 5.0 mg/kg, and butorphanol 0,2 mg/kg IM). Anesthesia was induced with propofol (10 mg/ml), then the pig was intubated and the anesthesia was maintained with an infusion of propofol 15 mg/kg/t and fentanyl 25-50 μg/kg/t. After the procedure, the pig was euthanized while still in anesthesia with an overdose of anesthetics (pentobarbital 135 mg/kg IV). Animal housing, care, and preparation were performed by qualified staff under the supervision of a designated veterinarian.

The second *in-vivo* experiment (Experiment 2) was conducted in collaboration with the medical team of the University of Queensland (UQ) under Ethics Approval UQCCR/GRIFFITH/406/20. Trained medical staff and a veterinary surgeon participated in the trial and were responsible for the implantation of the receivers and animal handling. A large female white pig (approximate weight of 23 kg with a waist circumference of 82 cm) was used in the experiment. Premedication was performed using 1.4mg/kg azaperone (Stresnil, Elanco, Australia) and 3.5 mg/kg ketamine IM (Ketamil, Troy Laboratories, Australia). Following premedication, induction was achieved through titration of alfaxalone (Alfaxan; Jurox Pty Ltd, AUS) into the lateral ear vein to a dose of 0.5 mg/kg IV. The pig was intubated using a size 7 mm cuffed endotracheal tube and anesthesia was maintained with 1.5-2% isoflurane (Henry Schein) in medical oxygen. Throughout surgery, anesthetic monitoring parameters included pulse oximetry, capnography, heart rate, respiratory rate, inspiratory and expiratory isoflurane concentrations (Masimo ISA AX+ Sidestream gas monitor was used for capnography, and a multigas monitor with Masimo Radical 7 Root monitor for pulse oximetry). Fluid replacement therapy was administered via the lateral ear vein at 9ml/kg/hr. Peri-anesthetic analgesia was provided with a combination of methadone (Methone 0.2 mg/kg IV) and ketamine (1 mg/kg IV); midazolam (0.2 mg/kg IV) and alfaxalone (0.25 mg/kg IV) were used to maintain consistent respiratory effort and reduce movement artefact. At the completion of the study protocol, euthanasia was performed using sodium pentobarbital (125 mg/kg) intravenously.

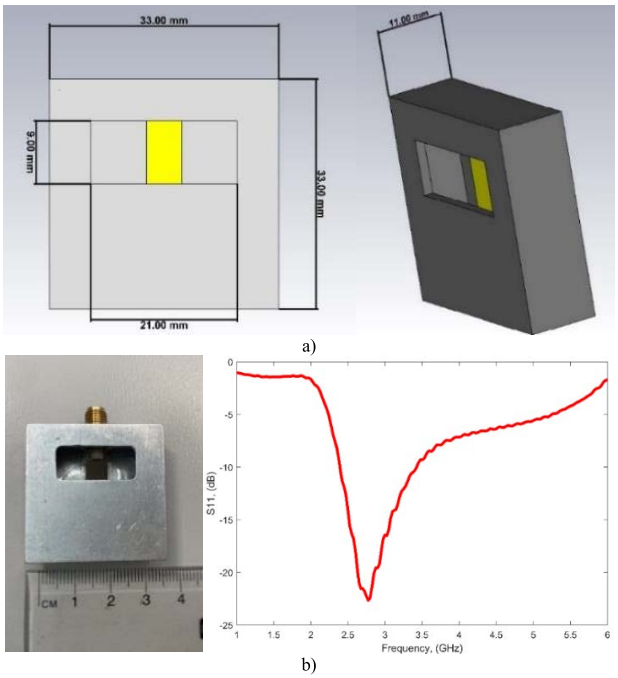

FIGURE 1. The receiver cavity-backed slot antenna design: (a) The antenna consists of a square aluminum box with a side of 33 mm and a thickness of 11 mm, the brass probe with the dimensions of 21.5 mm × 5 mm × 0.1 mm; the size of the slot is 21 mm × 9 mm [30] ©2021 John Willey & Sons, Inc; (b) Physical representation of the slot antenna on the left; The experimentally measured reflection coefficient S_{11} was −22.7 dB at 2.7 GHz with a bandwidth of 1.02 GHz, shown on the right.

Both experiments were designed as an internal transmitter to an external receiver channel (in-body to on-body) using the same RF measurement equipment, while the torso area represented a realistic propagation environment for WCE applications. A cavity-backed slot antenna used as a receiver was first reported in [29]. It was further modified for better performance as an on-body sensor and tested on various patients with different anthropometric parameters *in-vivo* [30]. Their study investigated the effect of the thickness of the abdominal wall layers, reporting that there was no significant effect observed that could affect the antenna performance.

The final design of the antenna consists of two main parts: a machined aluminum box with a rectangular slot and a monopole probe made of brass (Fig. 1). A brass probe placed perpendicular to the slot is connected to a coaxial cable via a 50 Ω SMA connector (SMA 8500-0000; RF Shop, Lonsdale, Australia). The dimensions of the antenna are given in Fig. 1 (a). The slot antenna performance as a receiving sensor with the transmitter surrounded by the *ex-vivo* porcine tissues was also tested [21] to confirm the suitability of the cavity-backed slot antenna for in-body to on-body measurements at 2.45 GHz. An example of the reflection coefficient measurements for the antenna when placed directly on the skin in the abdominal region of a living human is given in Fig. 1 (b). A resonant frequency of 2.7 GHz and a reflection

FIGURE 2. Experimental procedure: a) S_{11} Measurements taken for the on-body slot antenna using a Vector Network Analyzer (N9923A FieldFox). The slot antenna is oriented vertically (same was repeated for the mediolateral orientation). The transmitter was not implanted inside the abdominal cavity of the animal at this stage of the experiment; b) The RSSI was registered using the RF Explorer Spectrum Analyzer from the implanted Tx in the abdominal cavity. In this example, the on-body slot antenna is oriented mediolaterally (the same was repeated for all Rx positions for both orientations).

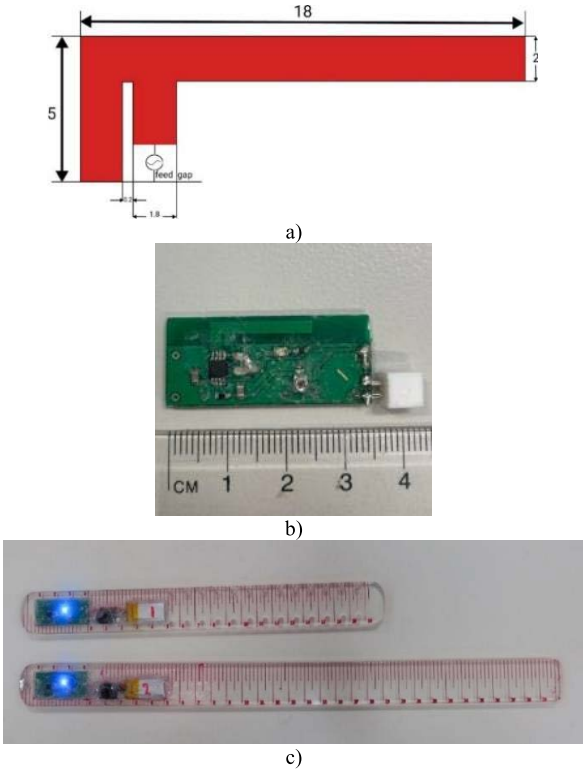

FIGURE 3. The IFA antenna with circuit used as an implantable transmitter in the experiments: a) Antenna layout and dimensions; b) Physical representation of the fabricated antenna with the ground plane on a substrate; c) Two insertion tools with variable length for different implantation depths. The LED always pointed towards the front of the animal in all experiments.

coefficient of −22.7 dB were observed. The −10 dB bandwidth of 1.02 GHz (42% of 2.45 GHz).

The primary goal of the experiments was to validate the attenuation path loss propagation model for the given in-to-on body communication scenario. They also served as a verification of the performance and applicability of the on-body slot antenna as a receiving sensor (Rx) for WCE localization in real-life conditions. The RSS and the antenna reflection coefficient (S_{11}) values were obtained across the frontal surface of the abdominal area of the animal. A Vector Network Analyzer (N9923A FieldFox Handheld RF VNA 6 GHz, Keysight Technologies ®, https://www.keysight.com) was used for S_{11} measurements as a part of the antenna performance evaluation. An RF Explorer Spectrum Analyzer (a handheld spectrum analyzer https://www.rf-explorer.com) was used for the RSS measurements to receive and display the maximum signal strength in dBm at 2.45 GHz. The values at each measurement point were manually recorded during the experiments. Fig. 2 shows the measurements taken on the skin of the animal (Experiment 2, the same RF equipment and the same procedures as were used in the first *in-vivo* experiment).

The ingested endoscopy capsule was imitated by a small inverted-F antenna (IFA) coupled to a battery-powered oscillator with the purpose of creating sufficient signal strength to be detected by the on-body slot antenna. It consists of a monopole placed parallel to a PCB ground plane with a short-circuit and a printed feed. The IFA design has good radiation efficiency and a small size, as the monopole is co-planar with the ground plane and the circuitry.

In [21], a conventional IFA design was optimized to match the characteristics of human soft tissues when implanted inside the abdominal cavity. The reported results on the skin surface demonstrated the antenna resonated at 2.45 GHz with a reflection coefficient of −13.3 dB. The dimensions of the IFA are given in Fig. 3. The dimensions of the ground plane were 35 mm×10 mm×0.02 mm and the monopole length was 18 mm. In both trials, the IFA Tx and the corresponding electronic components were fabricated on a PCB with an FR4 dielectric substrate (35 mm×20 mm×1.6 mm).

Additional modifications to the Tx antenna were made in order to have more control when manually positioning it inside the abdominal cavity of the animal. A custom-designed plastic insertion tool was made for the implantation. This device was manufactured by 3-D laser cutting on semi-rigid plastic with a thickness of 6 mm. The Tx and the battery were embedded close to the end of the insertion tool and were covered with an insulating silicone sealant (Fig. 3 [c]). The PCB circuit and the battery connector were additionally covered with a thin layer of plastic.

The insertion tool also served as a measuring device with a millimeter scale up to 30 cm, to control the distance from the entry point on the skin surface, while the depth from the frontal skin surface of the animal was determined by ultrasound measurements.

In Experiment 1, the real position of the Tx inside the abdominal cavity was determined with the use of an ultrasound imaging unit (Philips Healthcare, https://www.philips.co.uk/) with S3–1 (1–3 MHz) sector array and L12–3 (3–12 MHz) linear array transducers. In Experiment 2, a GE LOGIQe ultrasound unit (General Electric Healthcare,

a) b)

FIGURE 4. An example of ultrasound imaging measurements obtained during Experiment 2: a) An ultrasound probe on the surface skin of the laboratory animal placed in accordance with the marked grid; b) Transverse ultrasound image of the anterior abdominal wall of the animal and an indication showing the insertion tool with the transmitting antenna inside the abdominal cavity (arrow indicates the edge of the insertion tool while the Tx position in relation to the edge was predefined). The ultrasound imaging equipment had a precision of 0.1 mm.

a) b)

FIGURE 5. Tx implantation and measurements procedure: a) The in-house manufactured transmitter on the insertion tool was activated prior to implantation. It was implanted through an incision on the side of the pig in Experiment 2; b) Surface electric field measurements taken on the skin of anesthetized laboratory animal in Experiment 1. The measurement positions for the Rx were marked on the skin of the animal. The receiving slot antenna was placed in direct contact with the skin to detect the signal from the Tx.

https://www.gehealthcare.com) with a 5-MHz convex array transducer was used. In both trials, interpretation of the results was performed by trained ultrasound imaging specialists. The distance from the incision along the direction of the implantation was found using the scale on the insertion tool, which determined the 2-D location of the Tx along the predefined measurement grid marked on the skin of the animal (Fig. 4 [a]). Ultrasound imaging results obtained at that point provided an estimate of the depth from the skin surface of the animal to the edge of the insertion tool and the Tx correspondingly, giving its coordinate in the third dimension. The combination of these measured parameters allowed an estimate of the location of the Tx at a given point in 3-D space. An example of the ultrasound imaging results is given in Fig. 4 (b).

B. MEASUREMENT PROCEDURE AND DATA ANALYSIS

In both trials, the animal was placed on its back and the transmitting IFA Tx was surgically implanted through a small skin incision. After the implantation, the EM field strength was registered as RSSI in dBm at predefined positions by the receiving slot antenna (Rx).

Different locations of the Tx in the abdominal cavity were considered for the exploration of different signal path lengths. Following the field strength measurements on the skin surface of the animal for the first location of Tx, the insertion tool was withdrawn stepwise and the signal strength at each receiver position was recorded again at each step. The field strength measurements were conducted by positioning the Rx along a marked grid over the torso while connected to the Spectrum Analyzer (Fig. 5 b).

Apart from different animals being subjects in the trials, the measurement grid on the skin surface for Rx positions and the direction of the insertion tool implantation were different. In Experiment 1, the incision was made in the lower part of the abdominal area, while in Experiment 2 it was made on the side of the pig torso (Fig. 5). Therefore, different locations of the implanted antenna inside the abdominal cavity created different propagation paths. This enabled the difference in the insertion tool retrieval direction, meaning that in Experiment 1, the main change in the implanted antenna location was along the sagittal plane, while in Experiment 2, it was in the direction of the transverse plane. The muscle fibers in the abdominal region have directionality, which may have an effect on the signal propagation and the values of the measured surface signal.

For all measurements, the antenna PCB was parallel to the front surface of the animal. As the on-body slot antenna was linearly polarized, the measurements in both trials included two orientations of the slot antenna on the skin surface. Due to the high losses in the surrounding soft tissues of the animal, it was assumed that the implanted antenna behaved as a Tx with an omnidirectional radiation pattern. This assumption was tested as a part of both experiments.

The schematic representation of the Tx implantation at different locations is given in Fig.6 for each trial. In Experiment 1, the Tx on the implantation tool was first inserted towards the furthest possible point from the incision, and then withdrawn using the step size of 2.5 cm marked on the insertion tool (Fig. 6 [a]). The Rx was placed on the skin of the anesthetized pig at 17 predefined positions where the field strength was recorded (Fig. 6 [b]). The measurement grid dimensions were designed taking into consideration the size of the receiving slot antenna and the size of the frontal surface area along the abdominal cavity.

The measurement grid was expanded in Experiment 2 to create more data points for a more reliable validation of the PLM and a more comprehensive localization accuracy assessment. The incision was made laterally to control the position of the Tx better and to investigate a displacement of the Tx along the transverse plane. The extended measurement grid contained 30 Rx locations with a step-size of 3 cm (Fig. 6 [d]). In each of the experiments, four different Tx locations were created (Fig. 6 [a] and [c]).

To verify the performance of the slot antenna, the measurement grid on the skin of the animal had a configuration similar to the measurements assessing the antenna performance

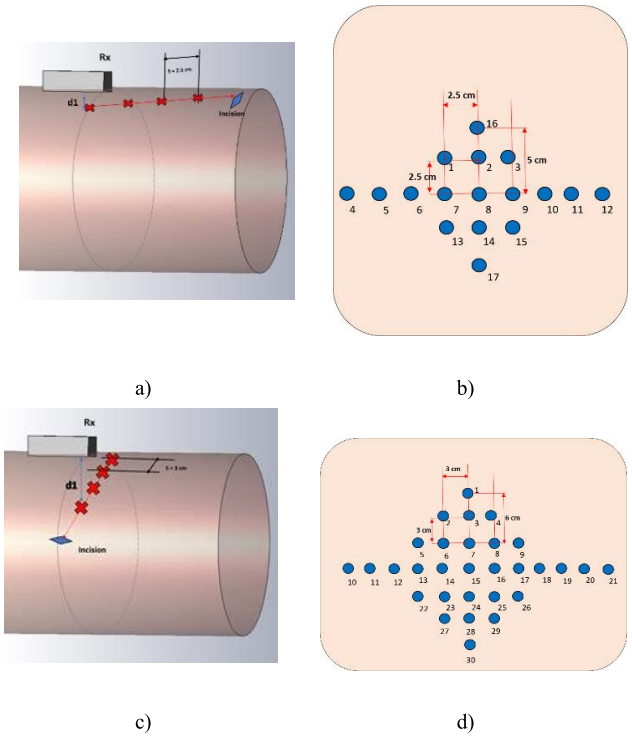

FIGURE 6. The representation of the Rx positions and four Tx locations: a) and c) Schematic representation of the tested position of the IFA inside the abdominal cavity, for Experiments 1 and 2 respectively; b) and d) The grid that represents all on-body measurement points for collecting the data, for Experiments 1 and 2 respectively.

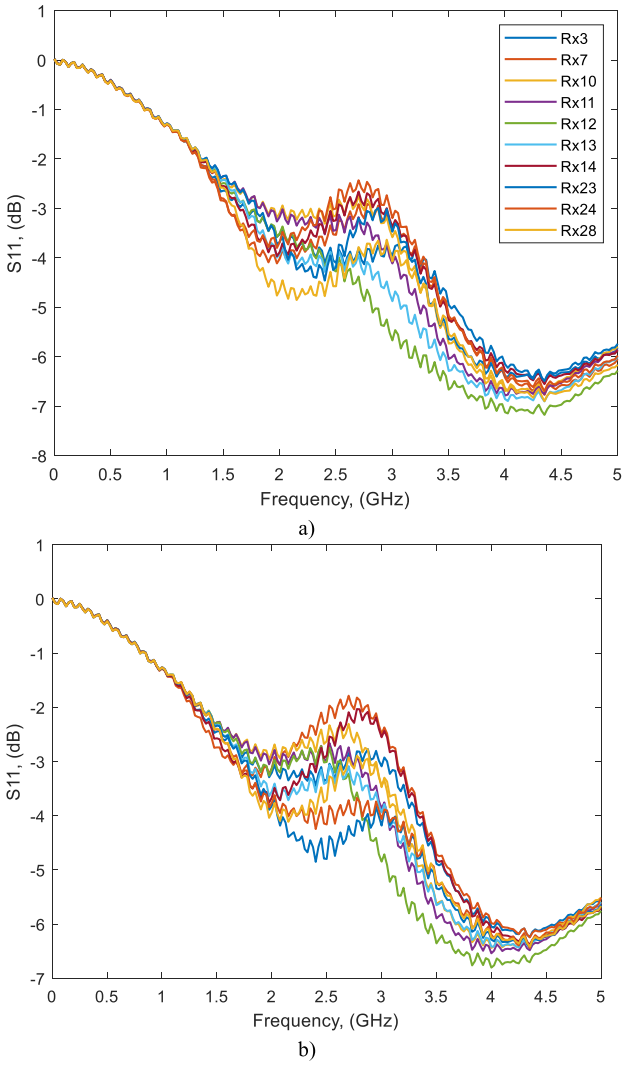

FIGURE 7. The S_{11} parameter measured for 10 of the Rx positions in Experiment 2 for the antenna oriented: a) mediolaterally and b) vertically along the torso of the animal. Note that the same legend applies to the results obtained in both orientations and that the numbers of the receivers given in the figure are in compliance with the measurement grid in Fig 6 (d).

on human subjects in prior research [30]. In Experiment 1, the Rx showed an average S_{11} value of -3.5 dB (standard deviation of 0.5 dB). In [30], measurements on humans were reported, suggesting that an S_{11} lower than -4 dB can be considered reasonable for reliable field strength measurements. In Experiment 2, the S_{11} parameter was measured for several Rx positions of the antenna using both orientations (10 values for each orientation). The results are presented in Fig. 7. The corresponding values were determined at 2.45 GHz: mean $=$ -3.1 dB (standard deviation 0.7 dB) for vertical orientation (Vert); mean $= -3.5$ dB (standard deviation of 0.5 dB) for mediolateral orientation (ML). The results are similar to those obtained during Experiment 1 and were considered to be well matched for the purpose of the study.

For the numerical analysis and evaluation of the PLM parameters, the torso of the animal was represented as an elliptical cylinder approximation using the real physical dimensions of the animal in both experiments. The elliptical model is a realistic geometric representation of the human body and the Rx and Tx locations in 3-D [31]. The radii of the cylinder were chosen to match the circumference of the model to the physical circumference of the pigs. The height of the cylinder was chosen to be the same as the elliptical cylinder model in the numerical validation of the attenuation algorithm for surface field reconstruction in [27]. Fig. 8 shows the elliptical cylinder reconstructed for the numerical results in Experiment 1.

The coordinate system was defined with the origin in the center of the elliptical cylinder. A symmetrical measurement grid representing Rx positions was created on the surface of the cylinder (x-z plane in 2-D) with the point of symmetry at Rx with the coordinates of [0 m, -0.13 m, 0 m] (Fig. 8 [a]). The y-coordinate of that Rx is equal to the elliptical radius in the sagittal plane, $r_y = 0.13$ m. The step between two consecutive Rx positions in both x and z directions was 0.025 m. Two datasets of signal strength values were obtained separately at positions with ML and Vert coordinates of the receivers from each of the transmitter locations shown in Fig. 8 as red dots. The data analysis accordingly considered the received results separately for ML and Vert. Note that

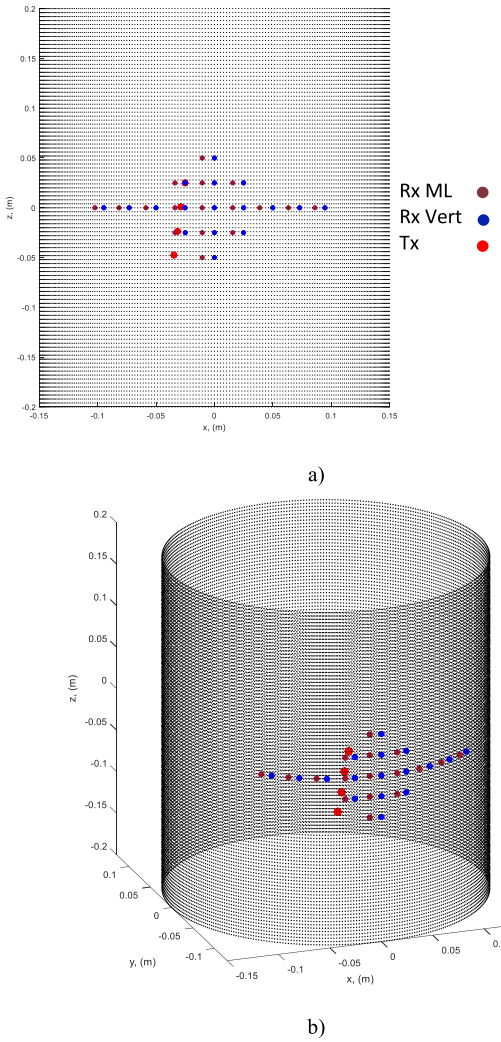

FIGURE 8. The elliptical cylinder model representing the coordinate systems in 2-D (a) and in 3-D (b) for the measurement analysis and the corresponding positions of the Rx and the Tx locations inside the abdominal cavity of the animal in Experiment 1 ($r_x = 0.15$ m and $r_y = 0.13$ m., z range: -0.2 m to 0.2 m). The Rx locations for two orientations are demonstrated in different colors.

for the mediolateral orientation, the measurement grid had a slight offset due to the measurement point at the center of the slot being placed to the left of the physically marked location on the skin. The implantation depth was represented by the y-coordinate. The main displacement for each of the Tx locations is along the z-axis, as it was the direction of the insertion tool withdrawal.

For the data analysis and calculations in Experiment 2, an elliptical cylinder approximation based on the physical dimensions of the animal described in Section III for the trial at the University of Queensland facilities, Brisbane, Australia, was used ($r_x = 0.15$ m and $r_y = 0.11$ m, Fig.9). As was the case for the first experiment, the implantation depth from the frontal surface was reconstructed in the y-axis direction within the model. Note that in Experiment 2, Rx measurement positions for both ML and Vert orientations

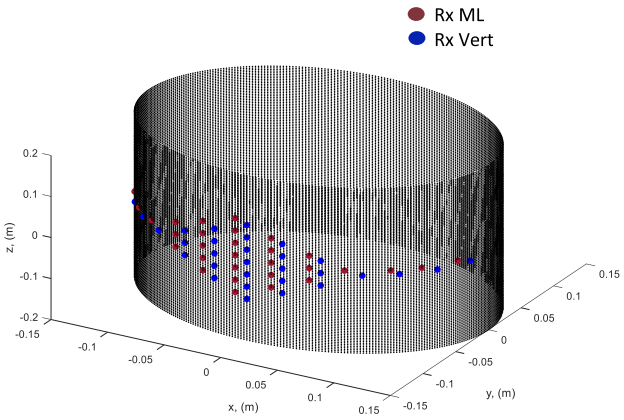

FIGURE 9. The elliptical cylinder model in 3-D and the corresponding positions of the measurement grid. The Rx locations for the two Rx antenna orientations used in Experiment 2 are shown in different colors. ($r_x = 0.15$ m, $r_y = 0.11$ m, $z = -0.2$ m to 0.2 m).

experienced an offset from the marked grid on the skin, hence the corresponding offset from the point of symmetry at [0 m, -0.11 m, 0 m].

Fig. 10 shows the Tx locations in the 3-D space of the model – the solution space for Experiment 2. The main change in the Tx location in this case was made along the x-axis following the direction of the insertion tool implantation. The retrieval step of the insertion tool starting from the maximum implantation (20 cm on the insertion tool) in the x-direction was 4 cm, resulting in four different locations of Tx as in the first experiment. The Rx measurement grid within the coordinate system of the numerical model varied for the ML and Vert orientations. Fig. 10 (a) shows the Rx in the Vert orientation with an offset of -0.01 m in the z-direction from the marked grid on the skin. The Rx for the measurements in the ML orientation were made with an offset of -0.01 m in the x-direction along the curvature of the cylinder model correspondingly in (Fig. 10 [b]). The step between two consecutive Rx positions in Experiment 2 in both x and z directions was 0.03 m.

The path length between each of the Tx locations and each of the Rx on the skin was estimated using the approximated 3-D coordinates given by the reconstructed numerical models. The described configurations of the transmitter and receiver positions resulted in 17×4 and 30×4 measurement data points in the first and second experiments, respectively (for each case, ML and Vert). Each defined a different path length or radial distance value and the corresponding RSS measurement that was registered during the experiments. Only data from positions that produced values above the noise level were used for the path model validation, which is described in detail in the following section.

IV. RESULTS AND DISCUSSION

A. INTENSITY DISTRIBUTION MAPS

The reconstruction of the RSS measurement grid in 2-D was used as a part of the preliminary analysis of the change in the intensity distribution of the surface electric field for different

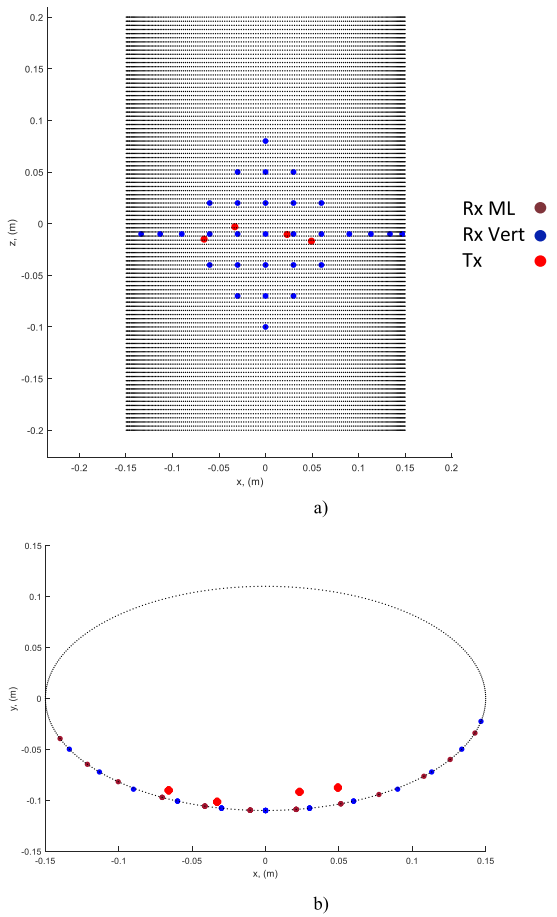

FIGURE 10. Different cross-sections of the elliptical cylinder model used as the solution space in Experiment 2: a) 2-D cross-section in x-z showing the measurement grid for the vertically (blue dots) oriented Rx antenna; red dots represent the changing Tx locations: Tx1, Tx2, Tx3, Tx4. The transmitter location was changed primarily along the x-direction by withdrawing the insertion tool with a step-size of 4 cm relative to the incision on the skin on the side of the animal. The tool was inserted along the x-axis. b) The elliptical cylinder model's surface curvature with the position of the Tx for each new location and corresponding Rx on the surface in ML and Vert orientations (brown dots, blue dots).

orientations of the slot antenna. The comparison between these results for each of the transmitter locations served as an investigation of the effect of the Tx orientation as well as the effect of slot antenna polarization.

The visual representation of the signal strength distribution across the skin surface of the animal was obtained by interpolating the results at each Rx position for a given Tx location. Fig. 11 and Fig. 12 demonstrate signal strength intensity maps for Experiment 1 derived from the acquired results at the 17 Rx positions for the slot antenna in both orientations: Vert – along the longitudinal or sagittal plane of the animal; ML – along the horizontal or transverse plane of the animal. The offset was -0.01 m for the ML case from the line of symmetry through the origin – along the x-axis in 2-D. The noise level for the data analysis of the results was approximately -92 dB.

For both orientations, the maximum intensity corresponds to the location of the Tx in each of the figures. Considering that the different Rx orientations produced different sets of the coordinates of the measurement points and that each of the Tx had different coordinates, the results confirm the assumption that there is a dependency between the radial distance and the obtained signal strength. It can be used to characterise a given Tx location for a known set of Rx. Moreover, no significant directionality was found between the distribution of the intensities around the maximum value when comparing ML and Vert orientations. This supports the assumption that the transmitting IFA sensor was omnidirectional for these *in-vivo* measurements.

Similar to the first experiment, a visual representation of the signal strength distribution was reconstructed by interpolating field strength (values in dB) obtained during Experiment 2 across 30 predefined positions of the Rx. Two datasets of the RSSI for the Rx in ML and Vert orientations were reconstructed separately, with the measurement grid offsets of -0.01 m along the x-axis and -0.01 m along the z-axis correspondingly (from the line of symmetry through (0,0) or the marked grid on the skin surface in real life). Fig. 13 and Fig. 14 demonstrate signal strength intensity maps for the acquired results for four Tx locations (Tx1, Tx2, Tx3, Tx4 but with different coordinates compared to the first experiment). Note that the same intensity scale has been used for comparison.

In Experiment 2, the results show a different signal strength distribution across the same measurement grid for each Tx location, as well as a slight difference in the maximum intensity positions across the solution space for the different Rx antenna orientations. This is explained by the significant change in radial distance that occurs when the Tx location inside the abdominal cavity is changed with respect to each of the fixed Rx. A slight offset in the Rx coordinates between the ML and Vert orientations resulted in a smaller radial distance change between the different orientations of the Rx but the same location of the Tx. The maximum field intensity follows the real location of the Tx very closely, although compared to the first trial, in this case the displacement of the Tx was mainly along the x-axis. The dispersion of the signal around the maximum when comparing ML and Vert orientations suggests that for this experiment the transmitting IFA sensor had an omnidirectional radiation pattern as in the first trial.

Since there was no significant difference observed in the results obtained by the slot antenna in different orientations in both experiments, we can conclude that the cavity-backed slot antenna does not experience any polarization effect.

B. APLM VALIDATION

The validation of the attenuation path loss propagation model suggested in this paper (8) involved an estimation of its parameters when experimental data from the two *in-vivo* trials were used separately. The performance metrics of the APLM were also assessed against the two other models described

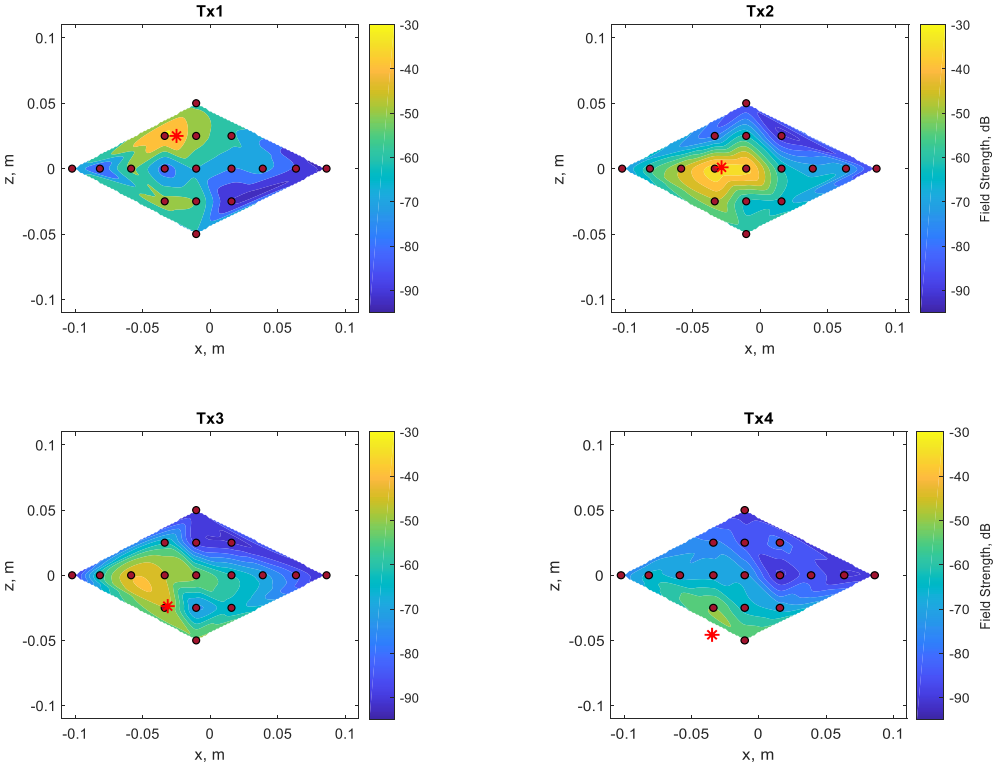

FIGURE 11. The distribution of electric field intensity across the measurement grid in 2-D in Experiment 1 for the four positions of the IFA-antenna (*, Tx1, Tx2, Tx3, Tx4) relative to the Mediolateral (ML) measurement positions of the Rx (red circles). Note that the intensity maps were created using interpolation between the measurement points, which explains the corresponding shape of the reconstructed results (no measurements were made beyond that area).

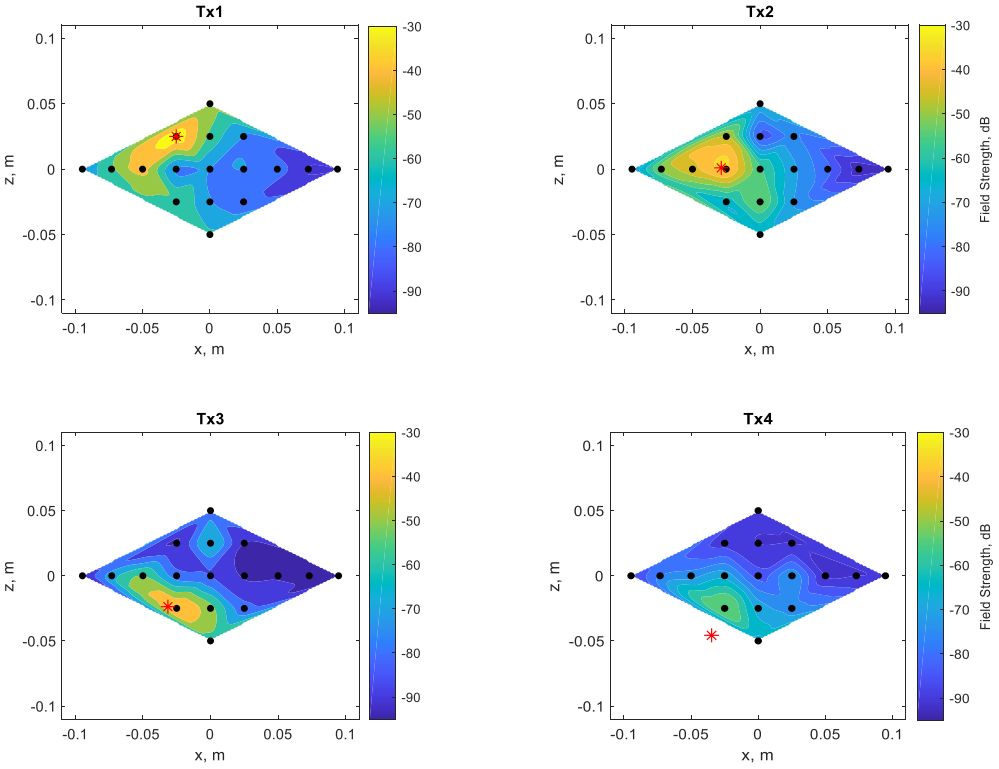

FIGURE 12. The distribution of electric field intensity across the measurement grid in 2-D in Experiment 1 for the four positions of the IFA-antenna (*, Tx1, Tx2, Tx3, Tx4) relative to the Vertical (Vert) measurement positions of the Rx (black circles). Note that the intensity maps were created using interpolation between the measurement points, which explains the corresponding shape of the reconstructed results (no measurements were made in the white space in the figures).

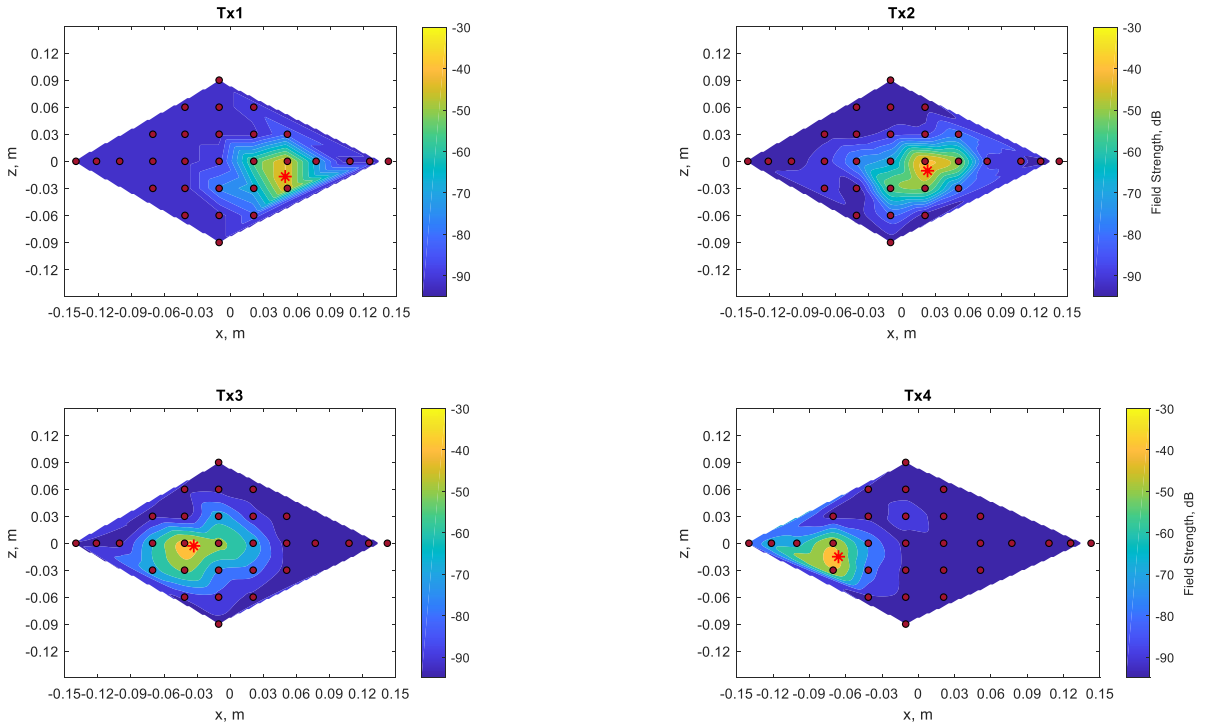

FIGURE 13. The distribution of electric field intensity across the measurement grid in 2-D in Experiment 2. The four positions of the IFA-antenna (*, Tx1, Tx2, Tx3, Tx4) were tested while the data was obtained by the Rx in the Mediolateral (ML) orientation (red circles). Note that the intensity maps were created using interpolation between the measurement points, which explains the corresponding shape of the reconstructed results (no measurements were made beyond that area).

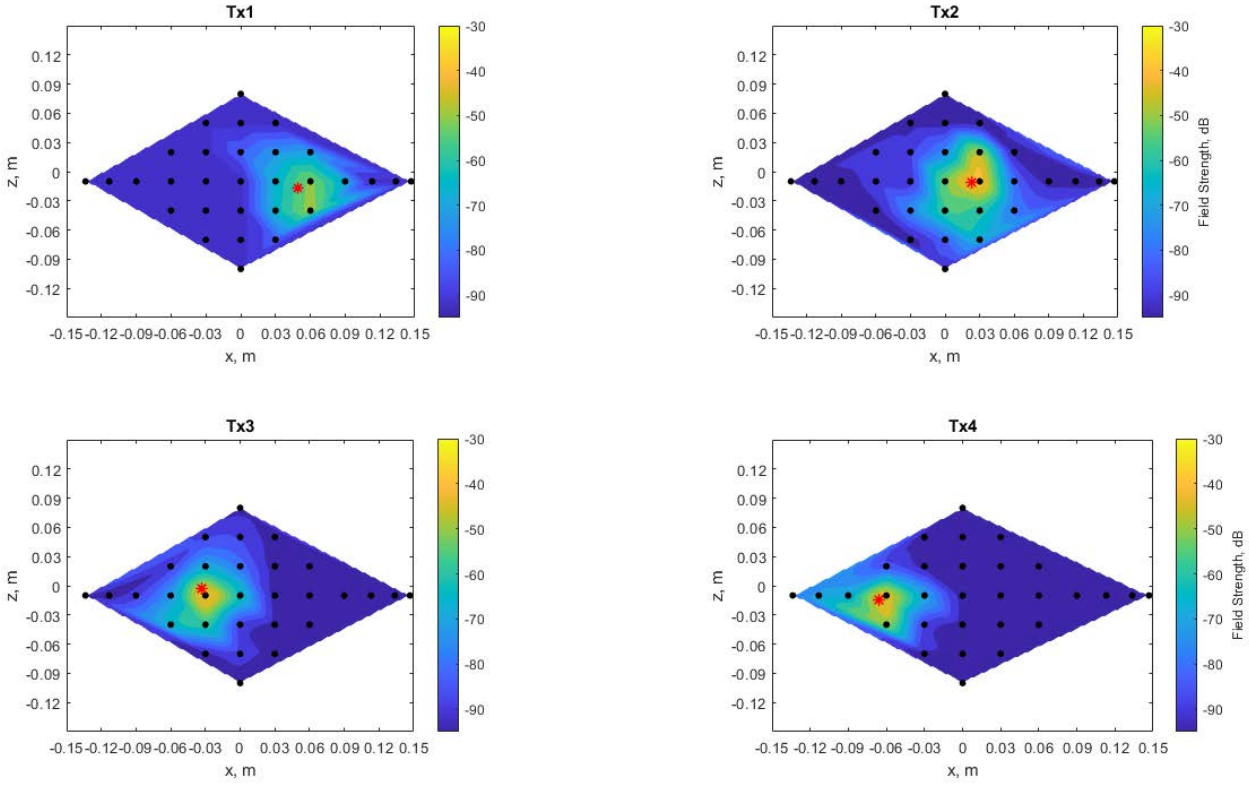

FIGURE 14. The distribution of electric field intensity across the measurement grid in 2-D in Experiment 2. The four positions of the IFA-antenna (*, Tx1, Tx2, Tx3, Tx4) were tested while the data was obtained by the Rx in the Vertical (Vert) orientation (black circles). Note that the intensity maps were created using interpolation between the measurement points, which explains the corresponding shape of the reconstructed results (no measurements were made in the white space in the figures).

TABLE 3. Parameters of the path loss models estimated using the Experiment 1 measurement data.

	APLM	Linear (plane wave)	Log-Distance
Mediolateral Rx Orientation			
α (Np/m) or n	59.59	72.08	6.7
C (dB)	60	28.8	151.4
RMSE (dB)	4.47	4.38	4.33
r^2	0.97	0.92	0.92
Vertical Rx Orientation			
α (Np/m) or n	65.65	82.7	7.26
C (dB)	60	25.88	159.6
RMSE (dB)	6.5	6.46	6.37
r^2	0.91	0.84	0.84

by (9) and (10). This required obtaining the corresponding coefficients for these models based on the same experimental data first and comparing them to the values reported in the literature, which are included in Table 2. These observations allowed to support the reliability of the findings of the current study.

The experimentally obtained parameters of the APLM, the attenuation coefficient in particular, were compared to the theoretical values of the EM properties of the human abdominal lossy tissues shown in Table 1. This was an important part of the validation, as the main novelty and advantage of the proposed model is its analytical basis that allows further generalization of the APLM for *in-vivo* measurements.

1) EXPERIMENT 1

The best-fit parameters of the three PLM and their performance metrics estimated when using the data obtained in Experiment 1 are given in Table 3. All three models perform equally well, although the best-fit parameters differ. This proves that the proposed APLM can perform as well as those reported in the literature, and even exhibit a slightly better correlation for both Rx antenna orientations.

When comparing the ML and Vert orientations, similar results were received for the APLM, including the same value of $C = 60$ dB and slightly different attenuation coefficients of 59.59 Np/m and 65.65 Np/m, respectively. Note that C is the constant defined in (8), and for the log-distance and the linear (plane wave) models it had a different values and was defined as C_2 and C_3 in (9) and (10), respectively.

When the Experiment 1 measurement data were fitted to the linear (plane wave) and the log-distance models, the estimated coefficients were similar to those reported in the literature. The linear model attenuation constant of 72.08 and 82.7 Np/m are close to the reported 67 and 87 Np/m by reference [14] Table 2 for the tissue-mimicking phantom experiments. The value of the path loss exponent obtained n of 7.26 and 6.7 in this study was similar to 10.6 reported by reference [16] Table 2 for the *in-vivo* measurements at 2.45 GHz.

TABLE 4. Ranging errors. Experiment 1.

	Mediolateral Rx Orientation	Vertical Rx Orientation
Average Absolute Error, (mm)	4.8	6.9
RMSE, (mm)	6.6	8.7
Relative Average Error, (%)	10.08	14.61

Fig.15 illustrates the APLM model fitted to the measurement data obtained during the Experiment 1 with the best-fit parameters mentioned in Table 3 for ML and Vert orientations, accordingly.

Considering that the main purpose of the APLM discussed in this paper is its implementation for WCE location estimation, it is important to investigate the corresponding ranging error when using the experimental values to find radial distances based on the received signal strength.

The ranging error is given in millimeters and is defined by a comparison between the real distances from the Tx to each of the Rx and the distance estimated using the APLM model. The calculations used for the average ranging error and the corresponding relative ranging error in percentage for each tested position are given as:

$$\textit{Average Ranging Error} = \frac{\sum_{i=1}^{N} \left| distance_{i,est} - distance_{i,real} \right|}{N}, \tag{11}$$

$$\textit{Relative Ranging Error} = \frac{\left| distance_{est} - distance_{real} \right|}{distance_{real}} * 100\%, \tag{12}$$

where $distance_{est}$ is the predicted radial distance, and $distance_{real}$ is the real radial distance between the Tx and a given Rx (N positions of Rx are considered, where N is a number of measurement points above noise).

Table 4 shows the ranging error values estimated when RSSIs obtained by the Rx in both orientations in Experiment 1 were used for radial distance estimation. The results demonstrate that the absolute ranging error was smaller for ML orientation of the Rx with a value 4.8 mm, while the Vert absolute ranging error was 6.9 mm.

Fig. 16 shows the distribution of the relative ranging error for both orientations when increasing the radial distance, with an average error of 10.08% and 14.61% for ML and Vert, respectively.

2) EXPERIMENT 2

The parameters of the path loss models estimated when analyzing measured RSSI in Experiment 2 are demonstrated in Table 5.

Similar to the first experiment, all three models perform equally well, while the correlation coefficient is slightly higher for the APLM proposed within this paper ($r^2 = 93.5$ for APLM, $r^2 = 0.88$ for the linear [plane wave] model, and $r^2 = 0.82$ for the log-distance model). These are the average correlation coefficients between the two orientations of

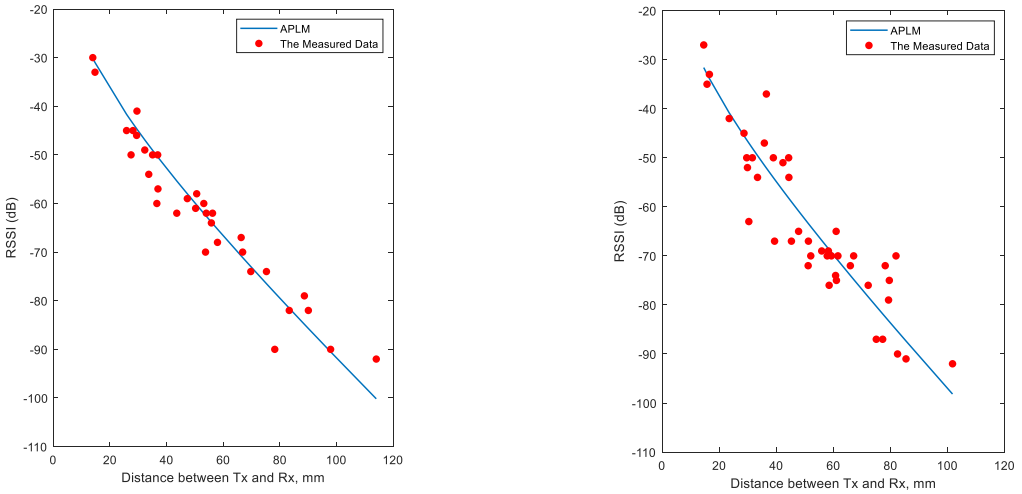

a) Mediolateral b) Vertical

FIGURE 15. APLM model fitted to the measurement data obtained during Experiment 1 with the best-fit parameters for ML and Vert orientations.

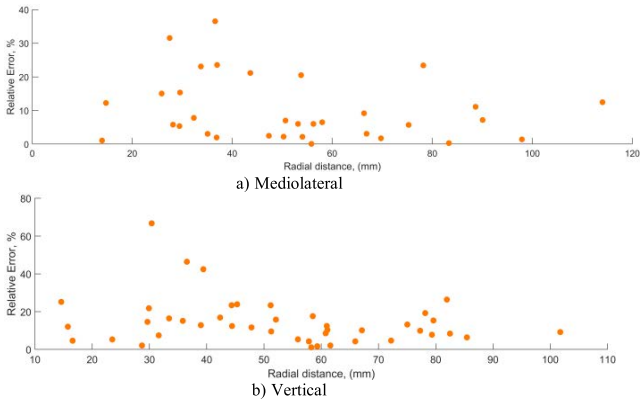

a) Mediolateral b) Vertical

FIGURE 16. Relative ranging errors when using APLM and the data obtained in Experiment 1: a) Mediolateral Orientation; b) Vertical Orientation.

TABLE 5. Parameters of the path loss models estimated using the Experiment 2 measurement data.

	APLM	Linear (plane wave)	Log-Distance
Mediolateral Rx Orientation			
α (Np/m) or n	73.73	98.13	7.72
C (dB)	63	24.9	151.4
RMSE (dB)	6.55	6.2	7.4
r^2	0.94	0.88	0.84
Vertical Rx Orientation			
α (Np/m) or n	73.73	104.62	6.94
C (dB)	67	26.98	163.94
RMSE (dB)	5.76	5.43	6.94
r^2	0.93	0.88	0.80

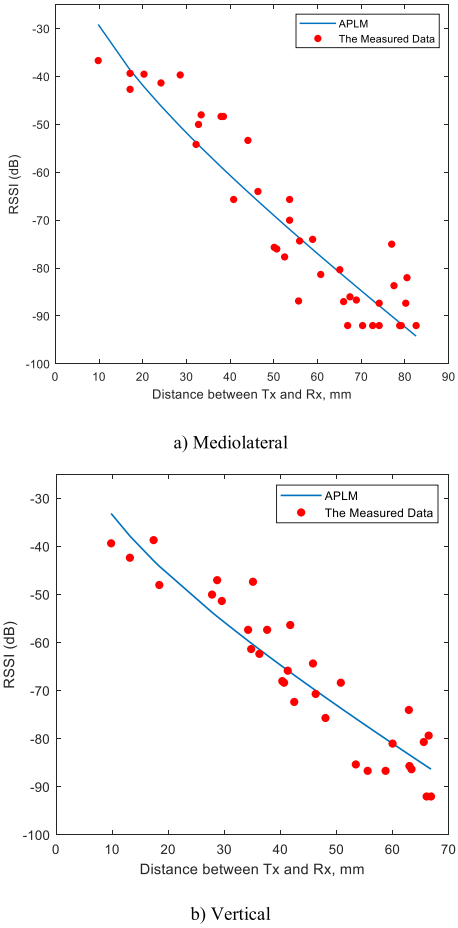

a) Mediolateral b) Vertical

FIGURE 17. APLM model fitted to the measurement data obtained during Experiment 2 with the best-fit parameters mentioned in Table 5 for ML and Vert orientations.

Rx for each model. When comparing each model to the corresponding results reported in the literature, the obtained values of the attenuation constant for the linear model 98.13 Np/m and 104.62 Np/m are close to 87 Np/m and 99 Np/m reported by references [14] and [15] Table 2 for the tissue-mimicking phantom experiments. The obtained value of the path loss exponent n of 7.72 and 6.94 in this study is similar to 10.6 reported by reference [16] Table 2 for the *in-vivo* measurements and the log-distance model.

Fig. 17 represents the measurement data obtained in Experiment 2 fitted to the APLM model.

TABLE 6. Ranging errors. Experiment 2.

	Mediolateral Orientation	Vertical Orientation
Average Absolute Error, (mm)	6.4	5.6
RMSE, (mm)	5.2	6.7
Relative Average Error, (%)	14.0	14.7

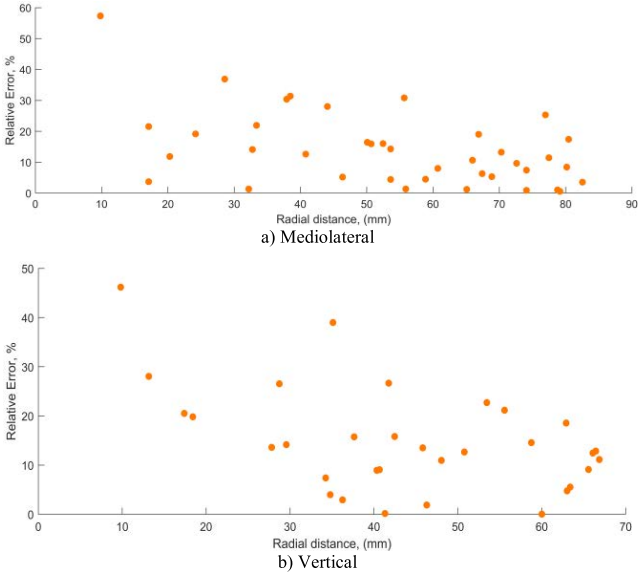

FIGURE 18. Relative ranging errors when using APLM and the data obtained in Experiment 2 by the Rx in: a) Mediolateral Orientation; b) Vertical Orientation.

The ranging errors given in Table 6 were estimated when using the APLM as the inverse solution for radial distance estimation, with the RSSI measured during Experiment 2 as the input values. The model parameters were chosen in accordance with the best-fit values given in Table 5. In this case, the absolute ranging error was smaller for the Vert of Rx with a value of 5.6 mm, while the mediolateral absolute ranging error was 6.4 mm. These results are consistent with the absolute ranging errors reported for Experiment 1 (Table 4).

Fig. 18 represents the distribution of the relative ranging error for both orientations of Rx in Experiment 2 with an increase in radial distance, with an average of 14.0% and 14.7% for ML and Vert, respectively.

C. DISCUSSION

All fitted parameters resulted in strong linear relationships between the APLM and the *in-vivo* measurements ($r^2 > 0.91$, Table 7), stronger than when the other models reported in the literature were fitted to the same experimental data. These observations support the reliability of the approach and the measurement equipment (the Rx slot antenna and the Tx antenna) for practical applications.

The attenuation coefficient is directly attributed to the EM properties of the abdominal soft tissues. An important observation is the close resemblance of the attenuation constant

TABLE 7. APLM parameters obtain in experiments discussed in the paper.

	α (Np/m)	C (dB)	RMSE (dB)	r^2
In-vivo (SDU), ML	59.6	60	4.47	0.97
In-vivo (SDU), Vert	65.7	60	6.5	0.91
In-Vivo (UQ), ML	73.7	63	6.55	0.94
In-Vivo (UQ), Vert	73.7	67	5.76	0.93

values estimated in both *in-vivo* experiments: 62.62 Np/m and 73.73 Np/m for the first and second trials (an average between two Rx orientations). These values are within the range of the theoretical α values for the human abdominal cavity organs reported in Table 1 for 2.45 GHz: 44.78 Np/m to 79.29 Np/m, an average of 58 (for the small intestine, colon, muscle, stomach, kidney). This demonstrated the reliability of the measurement system for practical applications in the signal propagation environment representing human tissues, and the reproducibility of the APLM parameters for several measurement trials. The latter supports the suggestion of further generalization of the APLM for WCE channel modelling.

This is enhanced by the fact that the constant C (dB) values representing the system performance characteristics were similar in both experiments: 60 dB and 65 dB for the first and second experiment, respectively. An average of 62.5 dB (standard deviation 3.32 dB) between the two trials can be estimated for the considered communications channel. The efficiency of the Tx and Rx and the directivity of the two antennas contribute to the value of the constant C (8).

It is noteworthy that the impedance of the slot antenna (S_{11}) on human subjects is similar to the measurements on anesthetized pigs. This provides additional validation that the pigs used in these experiments are relatively good human analogues.

The important parameter for the assessment of the APLM reliability as the inverse solution for range-based localization was the corresponding ranging error when the RSS values were used to find the radial distances. The average relative ranging errors (12.3% and 14.35%) were obtained in the first and second experiments, respectively, while the average absolute ranging errors were 5.85 mm and 6 mm (Tables 4 and 6). These findings point to the model's high reliability and accuracy, as well as the APLM's suitability for estimating the radial distance to an unknown implanted Tx in realistic scenarios.

V. CONCLUSION

Path loss propagation models serve as an important tool in wireless communication system design by enabling calculations of the received signal strength at a given distance. At the same time, they can be used to create an inverse solution using the given RSS value to determine an unknown distance between the sensors. This can be particularly useful for range-based localization problems. This

paper addressed radiofrequency-based localization of wireless endoscopy capsules as one of the relevant challenges that can benefit from the development of a suitable path loss propagation model. Wireless capsule technology is based on the transmission of an RF-signal from an antenna placed on an implanted sensor moving through the GI tract to the Rxs placed on the surface of the body. Although using the same RF-signal for the capsule localization could be beneficial, no standardized PLM exists that could be used for these purposes, especially for high operational frequencies.

This study discussed an alternative model to those reported in the literature. It includes an attenuation constant α instead of the path loss exponent as well as the spherical wave attenuation component. Such an approach is advantageous because it provides a correspondence to the real EM properties of the lossy human tissues. The validation of this model, referred to as APLM, was demonstrated through two separate experiments on living porcine animals, providing the most realistic conditions. The porcine abdominal visceral organs, intestine, and soft tissues in the abdominal cavity of pigs have similar EM characteristics to human tissue. The ability to conduct the measurements while the laboratory animals were under general anesthesia enabled data acquisition that incorporated the influence of natural movements, which can be present in the real-life application of the WCE. The estimated model coefficients of the APLM were similar for both trials. The values of the experimentally estimated attenuation coefficient parameter were close to the theoretical α values for the lossy human abdominal tissues. This confirmed the reliability of the model and its suitability to be used as a universal approach for similar propagation environments.

In future work, investigations on laboratory animals that have different EM properties could be beneficial in order to confirm that the proposed approach maintains its agreement with theoretical values in general. Apart from that, additional measurements when the implanted antenna is close to the tissues with significantly different conductivity, e.g., the bone structures, or when the latter form a part of the signal propagation path, could be conducted to demonstrate the change in the α values.

A comparison of the model performance characteristics to the similar or the most commonly reported in the literature validated on the same experimental data at 2.45 GHz, showed that the proposed APLM performed adequately, and even exhibited slightly higher correlation coefficients when predicting RSSI. An important characteristic in terms of the model accuracy is the ranging error obtained when using this model as an inverse solution to find the distance to a Tx. The reported absolute ranging error values in both of the trials were in the range of less than a centimeter. This can be considered a promising result for the further implementation of the APLM as a part of the range-based WCE localization. In future work, the corresponding positioning errors in 2-D and 3-D should be evaluated, to provide a more comprehensive analysis of the suitability of the proposed model for precise estimation of the unknown capsule location.

ACKNOWLEDGMENT

The authors would like to thank Stephanie Miller and Helen L. Keates (The University of Queensland, Brisbane, Australia), Dilani Mendis (Griffith University, Brisbane, Australia), and Diana Bianca Hansen and Laurfelt Munch Rasmussen (University of Southern Denmark, Odense, Denmark), who assisted in the experiments on living animals.

REFERENCES

[1] D. Silvera-Tawil, M. S. Hussain, and J. Li, "Emerging technologies for precision health: An insight into sensing technologies for health and well-being," *Smart Health*, vol. 15, Mar. 2020, Art. no. 100100.

[2] M. Puri, K. C. Chapalamadugu, A. C. Miranda, S. Gelot, W. Moreno, P. C. Adithya, C. Law, and S. M. Tipparaju, "Integrated approach for smart implantable cardioverter defibrillator (ICD) device with real time ECG monitoring: Use of flexible sensors for localized arrhythmia sensing and stimulation," *Frontiers Physiol.*, vol. 4, p. 300, Oct. 2013.

[3] H. Joo, Y. Lee, J. Kim, J.-S. Yoo, S. Yoo, S. Kim, A. K. Arya, S. Kim, S. H. Choi, N. Lu, H. S. Lee, S. Kim, S.-T. Lee, and D.-H. Kim, "Soft implantable drug delivery device integrated wirelessly with wearable devices to treat fatal seizures," *Sci. Adv.*, vol. 7, no. 1, Jan. 2021, Art. no. eabd4639.

[4] G. Iddan, G. Meron, A. Glukhovsky, and P. Swain, "Wireless capsule endoscopy," *Nature*, vol. 405, no. 6785, p. 417, May 2000, doi: 10.1038/35013140.

[5] C. Spada, C. Hassan, R. Marmo, L. Petruzziello, and M. E. Riccioni, "Meta-analysis shows colon capsule endoscopy is effective in detecting colorectal polyps," *Clin. Gastroenterol. Hepatol.*, vol. 8, no. 6, pp. 516–522, 2010.

[6] *IEEE Standard for Local and Metropolitan Area Networks—Part 15.6: Wireless Body Area Networks*, IEEE Standard 802.15.6-2012, Feb. 2012, pp. 1–271, doi: 10.1109/IEEESTD.2012.6161600.

[7] G. Lazzi, R. Lee, and K. S. Nikita, "Guest editorial for the special issue on wireless real-time health monitoring technology for personalized medicine," *IEEE Trans. Antennas Propag.*, vol. 67, no. 8, pp. 4946–4954, Aug. 2019.

[8] Y. Wang, S. Yoo, J.-M. Braun, and E. S. Nadimi, "A locally-processed light-weight deep neural network for detecting colorectal polyps in wireless capsule endoscopes," *J. Real-Time Image Process.*, vol. 18, no. 4, pp. 1183–1194, Aug. 2021.

[9] E. S. Nadimi, M. M. Buijs, J. Herp, R. Kroijer, M. Kobaek-Larsen, E. Nielsen, C. D. Pedersen, V. Blanes-Vidal, and G. Baatrup, "Application of deep learning for autonomous detection and localization of colorectal polyps in wireless colon capsule endoscopy," *Comput. Electr. Eng.*, vol. 81, Jan. 2020, Art. no. 106531.

[10] N. Patwari, J. N. Ash, S. Kyperountas, A. O. Hero, R. L. Moses, and N. S. Correal, "Locating the nodes: Cooperative localization in wireless sensor networks," *IEEE Signal Process. Mag.*, vol. 22, no. 4, pp. 54–69, Jul. 2005.

[11] H. T. Friis, "A note on a simple transmission formula," *Proc. IRE*, vol. 34, no. 5, pp. 254–256, May 1946.

[12] T. S. Rappaport, *Wireless Communications: Principles and Practice*, vol. 2. Upper Saddle River, NJ, USA: Prentice-Hall, 1996.

[13] K. Sayrafian-Pour, W.-B. Yang, J. Hagedorn, J. Terrill, and K. Y. Yazdandoost, "A statistical path loss model for medical implant communication channels," in *Proc. IEEE 20th Int. Symp. Pers., Indoor Mobile Radio Commun.*, Sep. 2009, pp. 2995–2999, doi: 10.1109/PIMRC.2009.5449869.

[14] D. Kurup, W. Joseph, G. Vermeeren, and L. Martens, "Path loss model for in-body communication in homogeneous human muscle tissue," *Electron. Lett.*, vol. 45, no. 9, p. 453, 2009, doi: 10.1049/el.2009.3484.

[15] D. Kurup, W. Joseph, G. Vermeeren, and L. Martens, "In-body path loss model for homogeneous human tissues," *IEEE Trans. Electromagn. Compat.*, vol. 54, no. 3, pp. 556–564, Jun. 2012, doi: 10.1109/TEMC.2011.2164803.

[16] P. A. Floor, R. Chávez-Santiago, and S. Brovoll, "In-body to on-body ultrawideband propagation model derived from measurements in living animals," *IEEE J. Biomed. Health Informat.*, vol. 19, no. 3, pp. 938–948, May 2015, doi: 10.1109/JBHI.2015.2417805.

[17] R. Chávez-Santiago, C. Garcia-Pardo, A. Fornes-Leal, A. Vallés-Lluch, G. Vermeeren, and W. Joseph, "Experimental path loss models for in-body communications within 2.36–2.5 GHz," *IEEE J. Biomed. Health Inform.*, vol. 19, no. 3, pp. 930–937, May 2015, doi: 10.1109/JBHI.2015.2418757.

[18] S. Perez-Simbor, C. Andreu, C. Garcia-Pardo, M. Frasson, and N. Cardona, "UWB path loss models for ingestible devices," *IEEE Trans. Antennas Propag.*, vol. 67, no. 8, pp. 5025–5034, Aug. 2019, doi: 10.1109/TAP.2019.2891717.

[19] K. Ito, K. Furuya, Y. Okano, and L. Hamada, "Development and characteristics of a biological tissue-equivalent phantom for microwaves," *Electron. Commun. Jpn. (I, Commun.)*, vol. 84, no. 4, pp. 67–77, 2001.

[20] D. Sharma, B. K. Kanaujia, V. Kaim, R. Mittra, R. K. Arya, and L. Matekovits, "Design and implementation of compact dual-band conformal antenna for leadless cardiac pacemaker system," *Sci. Rep.*, vol. 12, no. 1, pp. 1–17, Dec. 2022.

[21] N. Albadri, Y. A. Salchak, D. V. Thiel, and H. G. Espinosa, "E-field distribution in *ex-vivo* porcine skin layer from a subsurface UHF transmitter," in *Proc. 14th Eur. Conf. Antennas Propag. (EuCAP)*, Mar. 2020, pp. 1–5, doi: 10.23919/EuCAP48036.2020.9136021.

[22] T. Karacolak, R. Cooper, E. S. Unlu, and E. Topsakal, "Dielectric properties of porcine skin tissue and *in vivo* testing of implantable antennas using pigs as model animals," *IEEE Antennas Wireless Propag. Lett.*, vol. 11, pp. 1686–1689, 2012, doi: 10.1109/LAWP.2013.2241722.

[23] M. Barbi, "Location and tracking for UWB in-body communications in medical applications," Ph.D. dissertation, Instituto de Telecomunicaciones y Aplicaciones Multimedia Universitat Politécnica de Valéncia, Valencia, Spain, 2019.

[24] F. T. Ulaby, E. Michielssen, and U. Ravaioli, *Fundamentals of Applied Electromagnetics*, vol. 7. Upper Saddle River, NJ, USA: Pearson 2015.

[25] D. Kurup, M. Scarpello, G. Vermeeren, W. Joseph, K. Dhaenens, F. Axisa, L. Martens, D. Vande Ginste, H. Rogier, and J. Vanfleteren, "In-body path loss models for implants in heterogeneous human tissues using implantable slot dipole conformal flexible antennas," *EURASIP J. Wireless Commun. Netw.*, vol. 2011, no. 1, p. 51, Aug. 2011, doi: 10.1186/1687-1499-2011-51.

[26] S. H. Lee, J. Lee, Y. J. Yoon, and S. Park, "A wideband spiral antenna for ingestible capsule endoscope systems: Experimental results in a human phantom and a pig," *IEEE Trans. Biomed. Eng.*, vol. 58, no. 6, pp. 1734–1741, Jun. 2011.

[27] Y. A. Salchak, H. G. Espinosa, and D. V. Thiel, "Modeling the surface field from an ingested radio transmitter with an approximate attenuation model for gastroenterology investigations," *IEEE Trans. Biomed. Eng.*, vol. 67, no. 2, pp. 504–511, Feb. 2020.

[28] C. Gabriel, "Compilation of the dielectric properties of body tissues at RF and microwave frequencies," Dept. Phys., King's Coll London, London, U.K., Tech. Rep. AL/OE-TR-1996-0037, 1996.

[29] M. Fernandez, D. V. Thiel, A. Arrinda, and H. G. Espinosa, "An inward directed antenna for gastro-intestinal radio pill tracking at 2.45 GHz," *Microw. Opt. Technol. Lett.*, vol. 60, no. 7, pp. 1644–1649, 2018, doi: 10.1002/mop.31217.

[30] N. M. Albadri, J. A. Hides, H. G. Espinosa, and D. V. Thiel, "The effect of human tissue on field strength measurements *in vivo* using a resonant UHF cavity-backed slot antenna," *Bioelectromagnetics*, vol. 42, no. 4, pp. 284–295, 2021, doi: 10.1002/bem.22331.

[31] D. P. Chrissoulidis and J.-M. Laheurte, "Radiation from an encapsulated Hertz dipole implanted in a human torso model," *IEEE Trans. Antennas Propag.*, vol. 64, no. 12, pp. 4984–4992, Dec. 2016.

YANA A. SALCHAK (Graduate Student Member, IEEE) is currently pursuing the Ph.D. degree in biomedical and electrical engineering with Griffith University, Brisbane, QLD, Australia. Her work is supported by the Griffith University International Postgraduate Research Scholarship. She is also a recipient of personal education grant, the 2020 IEEE Antennas and Propagation Society, and the C. J. Reddy Grant for Graduate Students. Her research interests include biomedical engineering, wireless localization, pattern recognition, signal propagation analysis in human tissues, and wearable technology in STEM.

NOOR M. ALBADRI received the master's degree in electrical engineering from The University of Queensland, Australia, in 2016. She is currently pursuing the Ph.D. degree with the School of Engineering and Built Environment, Griffith University, Brisbane, QLD, Australia. Her research interests include the design and manufacture of wearable antennas and wireless sensors, electromagnetic wave propagation, UHF, and in-vivo and ex-vivo measurements.

TRACEY BJORKMAN received the Bachelor of Science degree and the Master of Philosophy degree from Griffith University, Brisbane, Australia, in 1994 and 1998, respectively, and the Ph.D. degree in neuroscience from The University of Queensland, Brisbane, in 2003.

She is currently a Senior Research Fellow and the Group Leader (Newborn Brain Injury and Repair) with the UQ Centre for Clinical Research, Faculty of Medicine, The University of Queensland. Her lab focuses on improving outcomes after newborn brain damage resulting from birth asphyxia, neonatal seizures, fetal growth restriction, and premature birth using the pre-clinical neonatal piglet model. Her research group aims to understand brain injury processes and to evaluate potential strategies to support clinical care of the newborn and to develop tools to inform diagnosis and assessment.

CORA LAU received the Bachelor of Veterinary Science degree (Hons.) and the Ph.D. degree in neurophysiology from The University of Queensland, Brisbane, Australia, in 2003 and 2013, respectively. After her bachelor's degree, she moved to Tasmania and practiced as a Small Animal Veterinarian for three years.

She is currently a Laboratory Veterinarian with The University of Queensland. She has been extensively working with many laboratory species, including rodents, zebrafish, sheep, pigs, rabbits, guinea pigs, quails, chickens, Xenopus frogs, and Australian marsupials. She is routinely involved with development of in vivo experimental designs, surgery, anesthesia, drug administration, and toxicological and post mortem examinations. Her notable 2020 outcomes include serving as an Expert Panel Member for indexing a veterinary anesthetic agent for use in minor species and involvement in the preclinical development of a molecular clamp-stabilized subunit vaccine for severe acute respiratory syndrome coronavirus 2. Her research focuses are in the field of zebrafish anesthesia and analgesia, in which she is supervising an RHD Master's Student.

ESMAEIL S. NADIMI (Senior Member, IEEE) received the M.S. degree in electrical engineering from the Sharif University of Technology, Tehran, Iran, in 2004, and the Ph.D. degree in electrical engineering and control system theory from Aalborg University, Aalborg, Denmark, in 2008.

He is currently a Professor in artificial intelligence and clinical machine learning with The Maersk McKinney Moller Institute, and the Faculty of Engineering, University of Southern Denmark, where he is also the Head of the Team of Applied AI and Data Science (AID) and the Technical Research Leader of the Danish Centre for Clinical AI (CAI-X). In 2011, he joined the School of Engineering and Applied Sciences (SEAS), Harvard University, where he worked for a year. His research interests include artificial intelligence, clinical machine learning and causal inference, noneinvasive medical robots, and green and renewable energy.

PETER BOLLEN was born in The Netherlands, in 1965. He received the B.Sc. degree in experimental zoology, in 1992 (Utrecht, The Netherlands), the M.Sc. degree in laboratory animal science, in 1994 (London, U.K.), and the Ph.D. degree during an industrial fellowship of the Danish Academy of Technical Sciences from the University of Southern Denmark. From 2001 to 2022, he was an Associate Professor and the Head of Department at the Biomedical Laboratory, University of Southern Denmark. Currently, he is a Full Professor at the Department of Experimental Medicine, University of Copenhagen. He is also a member of the Scandinavian Association of the Laboratory Animal Science and an Ad-Hoc Consultant of AAALAC. His research interests include improvement of anesthesia, analgesia, and optimization of housing and nutrition of experimental animals.

HUGO G. ESPINOSA (Senior Member, IEEE) received the bachelor's degree in electronics and telecommunications engineering from the Monterrey Institute of Technology and Higher Education, State of Mexico, Mexico, in 1998, the master's degree in electrical engineering from the University of São Paulo, São Paulo, Brazil, in 2002, and the Ph.D. degree *(summa cum laude)* in electrical engineering from the Technical University of Catalonia, Barcelona, Spain, in 2008.

He has been a Visiting Researcher with the Federal Polytechnic School of Lausanne, Lausanne, Switzerland, and a Postdoctoral Fellow with the School of Electrical Engineering, Tel Aviv University, Israel. Since 2014, he has been with the School of Engineering and Built Environment, Griffith University, Brisbane, QLD, Australia, where he is currently a Senior Lecturer in electronic engineering. His research interests include antennas and propagation, wireless sensor networks, electromagnetic separation of non-ferrous materials, inertial-magnetic sensors, wearable sensor technology for human monitoring, and engineering education. He is the Chair of the Microwave Theory and Techniques/Antennas and Propagation (MTT/AP) Joint Chapter of the IEEE Queensland Section. He is also an IEEE STEM Ambassador.

DAVID V. THIEL (Life Senior Member, IEEE) received the bachelor's degree in physics and applied mathematics from The University of Adelaide, Adelaide, SA, Australia, and the M.S. and Ph.D. degrees from James Cook University, Townsville, QLD, Australia.

He is currently an Emeritus Professor with the School of Engineering and Built Environment and the Director of the Radio Science Laboratory, Griffith University, Brisbane, QLD, Australia. He authored the book *Research Methods for Engineers* (Cambridge, U.K.: Cambridge University Press, 2014), and coauthored a book on *Switched Parasitic Antennas for Cellular Communications* (Norwood, MA, USA: Artech House, 2002). He has authored six book chapters, over 140 journal articles, and coauthored more than nine patent applications. His research interests include electromagnetic geophysics, sensor development, electronics systems design and manufacture, antenna development for wireless sensor networks, environmental sustainability in electronics manufacturing, sports engineering, and mining engineering. He is a fellow of the Institution of Engineers, Australia, and a Chartered Professional Engineer in Australia.